doi:10.1016/S0022-2836(02)00739-8 available online at http://www.idealibrary.com on IDEAL® J. Mol. Biol. (2002) 322, 425–440

JMB

Detection and Characterization of Xenon-binding Sites in Proteins by ^{129}Xe NMR Spectroscopy

Seth M. Rubin[1,2], Seok-Yong Lee[2,3], E. Janette Ruiz[1,4] Alexander Pines[1,4] and David E. Wemmer[1,2,3]*

[1]*Department of Chemistry MC-1460, University of California, Berkeley B84A Hildebrand Hall Berkeley, CA 94720-1460, USA*

[2]*Physical Biosciences Division Lawrence Berkeley National Laboratory, 1 Cyclotron Rd Berkeley, CA 94720, USA*

[3]*Graduate Group in Biophysics University of California Berkeley, CA 94720, USA*

[4]*Material Sciences Division Lawrence Berkeley National Laboratory, 1 Cyclotron Rd Berkeley, CA 94720, USA*

**Corresponding author*

Xenon-binding sites in proteins have led to a number of applications of xenon in biochemical and structural studies. Here we further develop the utility of ^{129}Xe NMR in characterizing specific xenon–protein interactions. The sensitivity of the ^{129}Xe chemical shift to its local environment and the intense signals attainable by optical pumping make xenon a useful NMR reporter of its own interactions with proteins. A method for detecting specific xenon-binding interactions by analysis of ^{129}Xe chemical shift data is illustrated using the maltose binding protein (MBP) from *Escherichia coli* as an example. The crystal structure of MBP in the presence of 8 atm of xenon confirms the binding site determined from NMR data. Changes in the structure of the xenon-binding cavity upon the binding of maltose by the protein can account for the sensitivity of the ^{129}Xe chemical shift to MBP conformation. ^{129}Xe NMR data for xenon in solution with a number of cavity containing phage T4 lysozyme mutants show that xenon can report on cavity structure. In particular, a correlation exists between cavity size and the binding-induced ^{129}Xe chemical shift. Further applications of ^{129}Xe NMR to biochemical assays, including the screening of proteins for xenon binding for crystallography are considered.

Keywords: hydrophobic cavities; ligand–protein interactions; xenon binding; multiple isomorphous replacement; protein conformation assay

Introduction

The affinity of xenon for hydrophobic cavities in macromolecular interiors[1] has motivated a variety of applications of this inert gas in biochemical and structural studies of proteins. Xenon has been used to identify protein active sites and identify cavities that might be part of pathways by which substrates reach active sites.[2–4] Because of its small size and large polarizability, xenon has been used as part of model systems in both theoretical and experimental studies of ligand–protein binding.[5–7] A recent investigation demonstrated the ability of xenon to catalyze enzymatic reactions with radical pair intermediates.[8] In addition, there has been increasing use of xenon for determining phases in protein X-ray crystallography by both multiple isomorphous replacement (MIR) and multi-wavelength anomalous diffraction (MAD) techniques.[9–13] Despite the numerous ways investigators can employ specific xenon–protein interactions, there exists no simple assay for xenon binding. Here we further develop the use of ^{129}Xe NMR to detect protein cavities that bind xenon and explore using ^{129}Xe as a reporter of cavity structure.

The sensitivity of the ^{129}Xe chemical shift to its local chemical environment[14] has motivated the use of xenon as an NMR probe of biomolecules.[15–17] Exploiting intense optically pumped ^{129}Xe NMR signals,[18,19] it has been possible to probe cavities in lyophilized lysozyme and lipoxygenase,[20] detect blood oxygenation levels,[21] and identify ligand-binding sites in a lipid transfer protein[22] through the spin-polarization induced nuclear Overhauser effect.[23] With a functionalized cage, laser-polarized xenon was used to detect a ligand binding event.[24] The chemical shift of xenon in solution with the maltose binding protein (MBP) was shown to be sensitive to the conformation of the protein.[25] Although these studies have demonstrated that the ^{129}Xe shift changes in different protein environments, the detailed mechanism for these changes remains elusive. Here we examine ^{129}Xe chemical shift changes upon binding to hydrophobic cavities

Abbreviations used: MIR, multiple isomorphous replacement; MBP, maltose binding protein.

E-mail address of the corresponding author: dewemmer@lbl.gov

0022-2836/02/$ - see front matter

in proteins. By correlating NMR data with crystal structures, the influence of specific xenon–protein interactions on the ^{129}Xe shift is revealed. We find that the presence of a xenon-binding site can be deduced from ^{129}Xe chemical shift data alone and that the shift of xenon in such a site is affected by cavity structure. The implications of these findings for applications of xenon as a biomolecular probe are considered.

^{129}Xe chemical shifts in protein solutions

Tilton & Kuntz first described the behavior of the ^{129}Xe NMR signal of xenon in solution with myoglobin.[16] They observed a single resonance, reflecting fast exchange between xenon in water and xenon bound to a site in the protein that had been identified in previous crystal structures, and characterized the chemical shift as a weighted average of the shifts of xenon in these two environments. Non-specific xenon–protein interactions were later shown to affect the ^{129}Xe shift in myoglobin solution,[26,27] resulting in a complex pattern of up- and downfield shifts as a function of xenon and myoglobin concentrations. For all proteins studied there has only been a single ^{129}Xe resonance observed, with a chemical shift reflecting fast exchange of xenon among all specific and non-specific binding sites.[20,25,27,28] Titration of ^{129}Xe solutions with amino acid residues, peptides, and denatured proteins results in a downfield shift, linear in solute concentration, that results from non-specific interactions.[28] The concentration-normalized change in chemical shift, denoted as α and expressed in units of ppm per mM, depends on properties of the solute such as chemical functionality, charge, and size. The α values of denatured proteins increase linearly with the number of amino acid residues in the primary sequence with a slope approximately equal to 0.005 ppm mM^{-1} per amino acid residue.

With the exception of myoglobin, titrations of xenon solutions with native proteins have all resulted in downfield shifts in the ^{129}Xe signal that are linear with increasing protein concentration.[25,28] Despite the fact that unfolded proteins have more surface area exposed for non-specific xenon interactions, the α values of several native proteins (e.g. bovine serum albumin and unliganded MBP) are greater than for their denatured forms. It was suggested that this discrepancy arises from specific binding interactions in the native proteins that contribute to the ^{129}Xe chemical shift.[28] We report here the structure of MBP in the presence of xenon and confirm that, as anticipated by the α value, the protein binds xenon in an interior cavity. Changes in xenon affinity for this cavity upon addition of maltose can account for the sensitivity of the ^{129}Xe chemical shift to the conformation of MBP.

The fact that many specific and non-specific interactions contribute to the α value of a native protein makes it difficult to determine the effects on the ^{129}Xe chemical shift of particular specific binding sites. We examined the effects of a single interaction by comparing α values for phage T4 lysozyme with a xenon-binding site created or blocked by mutation or competitive binding. In this case, all xenon–protein interactions remain the same except at the cavity of interest. This approach follows the work of Tilton & Kuntz, who observed changes in the ^{129}Xe shift in myoglobin solution upon addition of HgI^{-3}, which blocks xenon binding.[16] The set of T4 lysozyme mutants described by Matthews and co-workers is an ideal system for such mutation and binding inhibition studies.[29] Cavities created by mutations of bulky hydrophobic residues bind xenon, and the structures of these complexes have been determined by X-ray crystallography.[7] By comparing the α values of these different proteins in the presence and absence of xenon inhibitors, the effects of the various cavity structures on the ^{129}Xe chemical shift can be elucidated.

Results

^{129}Xe chemical shifts of xenon in MBP solution

Addition of buffer with laser-polarized xenon to protein solutions enables rapid acquisition of ^{129}Xe NMR spectra for chemical shift determination. Figure 1 shows a series of spectra of 1 mM xenon dissolved in solution with MBP at varying concentrations. Each spectrum is from a single acquisition with a total time for data collection of less than 5 minutes. The xenon line width increases with protein concentration. This broadening has been observed in other protein solutions and results from exchange of xenon between sites in the protein (both non-specific and specific) and the solvent.[16,27,28] The decrease in signal with increasing protein concentration is due to increased spin–lattice relaxation of the xenon through protein protons, causing a loss of polarization during the time required to place the sample in the probe for data acquisition. At these concentrations of MBP and xenon, the resonance line width is modest (less than 0.2 ppm), which allows for measurement of the chemical shift with an estimated error of <0.02 ppm. As seen in the spectra and Figure 1(b), increasing protein concentrations shift the ^{129}Xe resonance downfield relative to xenon in buffer; the measured slope of $\alpha = 2.5 \pm 0.1$ ppm mM^{-1} is similar with that reported.[25]

The ^{129}Xe chemical shifts of 4 mM xenon in MBP solutions are also plotted in Figure 1(b). The slope of the titration at 4 mM xenon ($\alpha = 2.4 \pm 0.1 \times$ ppm mM^{-1}) is similar to that at 1 mM xenon. The lack of xenon concentration dependence of α indicates that only a small fraction of the xenon interacts with any particular site in the protein (see Discussion). The third titration plotted in Figure 1(b) is for 10 mM xenon with denatured MBP; the slope ($\alpha = 1.3 \pm 0.1$ ppm mM^{-1}) is less than

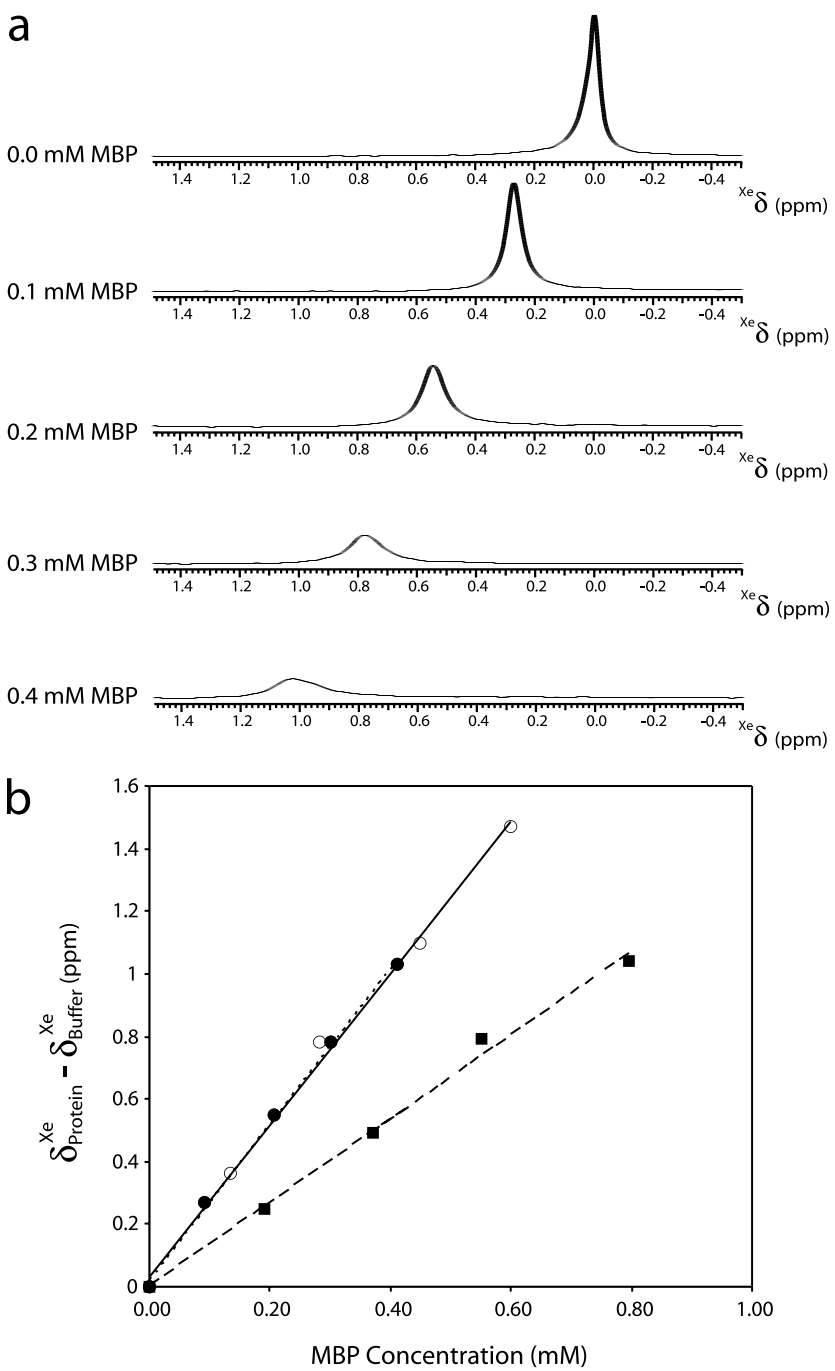

Figure 1. Effects of the MBP on ^{129}Xe chemical shifts. (a) ^{129}Xe NMR spectra of 1 mM xenon in solution with MBP at varying concentrations. The changes in ^{129}Xe chemical shift and resonance line width result from increased xenon–protein interactions with concentration. (b) ^{129}Xe chemical shift titration data for 1 mM (●) xenon and 4 mM xenon (○) in solution with MBP under native conditions and 10 mM in solution with MBP under denaturing conditions (■). The slope of both titrations under native conditions are similar ($\alpha = 2.5 \pm 0.1$ ppm mM^{-1} for 1 mM xenon and $\alpha = 2.4 \pm 0.1$ ppm mM^{-1} for 4 mM xenon), indicating that a small fraction of xenon interacts with any one protein site. The fact that the slope under denaturing conditions ($\alpha = 1.3 \pm 0.1$ ppm mM^{-1}) is less than under native conditions suggests the presence of a specific xenon-binding site. The reported ^{129}Xe chemical shifts for each titration are referenced to the shift of xenon in buffer.

the slope of the native titrations. The α value for denatured MBP is less than that anticipated by previous studies of denatured proteins on the basis of the number of amino acid residues in the polypeptide; however, deviations from the average value should be expected as contributions to the ^{129}Xe chemical shift from non-specific interactions will depend on the amino acid residue composition of the chain.[28]

Crystal structure of MBP pressurized with xenon

Considering non-specific interactions alone, the accessibility of more residues to xenon interactions in denatured MBP should result in an α value that is greater than that measured for native MBP. However, as seen in Figure 1, the measured α value of MBP is greater under native conditions. We previously suggested that this behavior in other proteins was caused by the presence of specific, higher affinity interactions that also contribute significantly to the ^{129}Xe chemical shift.[28] In order to demonstrate the presence of a xenon-binding site in MBP, we solved the crystal structure of the protein without maltose to 1.8 Å resolution in the presence of xenon. As previously described, unliganded MBP crystallized in the space group *P*1 with one molecule in the unit cell.[30,31] Crystals pressurized with 8 atm of xenon

Table 1. Crystallographic data collection and refinement statistics

Crystal	
Space group	*P*1
Cell dimensions *a*, *b*, *c* (Å)	38.2, 44.0, 57.6
Cell dimensions α, β, γ (deg.)	100.7, 101.4, 102.6
Data collection (cryogenic)	
Resolution limit (Å)	17.07–1.80
Measured reflections	55,908
Unique reflections	29,855
R_{sym} (%)	2.9
Completeness (%)	92.3
Average *B*-factor (Å^2) (Wilson 1.8–3.0 Å)	16.9
Refinement	
No. of molecules in AU	1
No. of amino acid residues	370
No. of solvent	172
Resolution used	17.07–1.80
Sigma cutoff	0.0
No. of reflections work/test	28,283/1472
Final *R*-factor/R_{free} ($\|F\| > 0\sigma$) (%)	20.4/22.6
Average *B*-factor (Å^2)	22.5
Highest resolution bin	1.80–1.91
Completeness highest resolution bin	76%
R-factor/R_{free} highest resolution bin	24.1/25.8
RMS deviations from ideal geometry	
Bond length (Å)	0.010
Bond angles (deg)	1.4

for 15 minutes were isomorphous to those previously used to solve the structure of unliganded MBP (PDB code 1OMP).[30] The data collection and refinement statistics are summarized in Table 1.

Figure 2 shows a difference electron density map calculated with $\|F_{obs,\,Xe}| - |F_{obs,\,native}\|$ using native structure factors and phases from the published structure (1OMP).[30] Only one significant peak is present, with a height of 5σ, consistent with a single xenon atom. The occupancy of xenon in the final refined model is 0.5. The xenon-binding site, shown in Figure 3, is located in the N-terminal domain just below the surface of the sugar-binding cleft that is in contact with the reducing glycosyl unit in the maltose-bound structure. Table 2 lists the protein atoms that delimit the cavity and the distances between these atoms and xenon. A water molecule and lysine side-chain lining the cavity indicate the proximity of the cavity to the surface. This feature of the cavity is less common among xenon sites in proteins, most of which are more deeply buried.[32] In the closed, maltose-bound state, the lysine forms two hydrogen bonds to the sugar.[33] The water molecule is relatively well-ordered (refined *B*-factor = 18 Å^2) and also appears in the open native structure.[30] The bound xenon is localized in the cavity away from the lysine and water at the protein surface.

Comparison of the xenon-bound structure with the native protein structure (1OMP) reveals little change in the position of the residues lining the binding cavity. The root-mean-square deviation (RMSD) between the side-chain atom positions of these residues (listed in Table 2) in the two structures is only 0.25 Å. For comparison, the RMSD between these same atoms in two MBP structures in the Protein Data Bank that have the same "open" conformation (1OMP and 1MPC) is 0.24 Å. The small perturbation in structure upon binding xenon is similar to what has been found in many proteins[32,34] and is consistent with the isomorphism of the crystals in the absence and presence of 8 atm xenon.

Affinity of xenon for MBP changes with protein conformation

While the α values of MBP in the absence of ligand and bound to β-cyclodextrin are similar, the α value of the maltose–MBP complex is significantly less.[25] Comparison of the X-ray structures of unliganded MBP and the maltose complex revealed a conformational change characterized as a rigid-body hinge bending between the two domains of the protein.[30,33] While binding of maltose induces the change from the open to "closed"

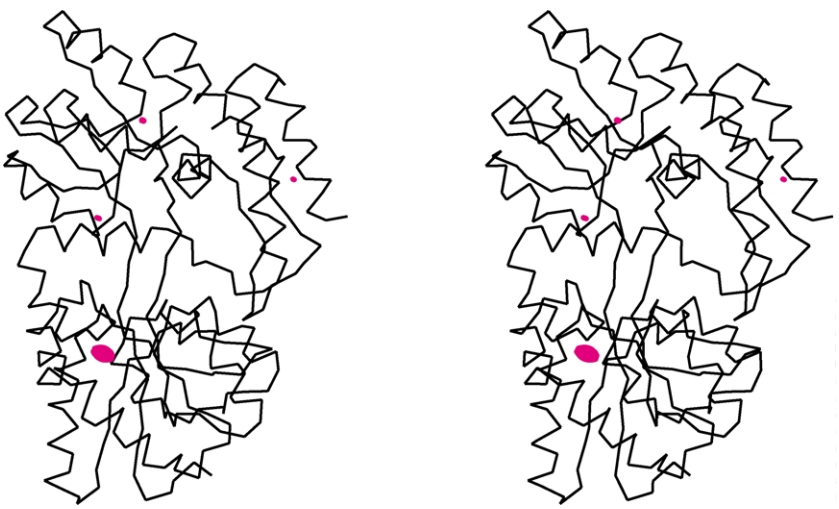

Figure 2. Stereo diagram of MBP with bound xenon. The density shown in magenta marks the difference Fourier map (contoured at 5σ) generated from the previously published native data set and the data set presented here for MBP crystals pressurized with 8 atm xenon. The xenon-binding cavity is located in the N-terminal domain of the protein below the surface of the sugar binding cleft.

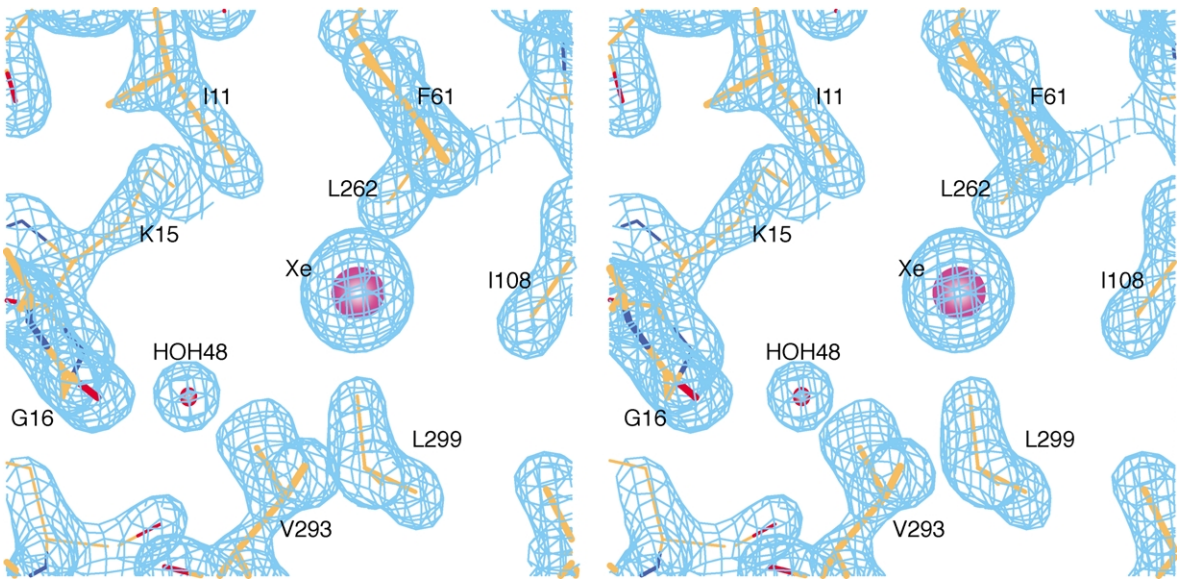

Figure 3. Stereo view of the xenon-binding cavity in MBP. The electron density in cyan corresponds to a $2F_{obs} - F_{calc}$ map contoured at 2σ. The xenon is localized in the cavity away from the lysine and water that mark the end of the cavity at the protein surface. While the presence of many hydrophobic side-chains is often observed in xenon-binding cavities, the proximity of the cavity to the surface is less common.

structure, both X-ray and solution NMR data have demonstrated that the conformation in the β-cyclodextrin complex more closely resembles the open unliganded structure.[35,36] This structural information with the ^{129}Xe NMR data suggests that the difference in α values results from the change in conformation. To test whether the affinity of xenon for the binding site in our crystal structure changes with conformation, we characterized xenon binding to MBP in the presence of β-cyclodextrin and maltose by heteronuclear NMR.

Table 2. Distances from xenon to neighboring atoms in MBP

Residue	Atom	Distance to Xe (Å)
ILE11	C^{γ_1}	5.3
ILE11	C^{δ_1}	3.8
LYS15	C^{β}	5.9
LYS15	C^{γ}	6.4
GLY16	O	6.0
LEU20	C^{α}	6.0
LEU20	C^{β}	5.1
LEU20	C^{γ}	5.0
LEU20	C^{δ_1}	4.3
LEU20	C^{δ_2}	4.7
PHE61	C^{β}	5.5
PHE61	C^{γ}	4.7
PHE61	C^{δ_1}	5.3
PHE61	C^{δ_2}	3.8
PHE61	C^{ϵ_1}	5.1
PHE61	C^{ϵ_2}	3.6
PHE61	C^{ζ}	4.3
ILE108	C^{β}	5.1
ILE108	C^{γ_1}	5.1
ILE108	C^{γ_2}	4.1
ILE108	C^{δ_1}	5.5
LEU262	C^{γ}	5.5
LEU262	C^{δ_1}	6.3
LEU262	C^{δ_2}	4.6
LEU284	C^{γ}	5.0
LEU284	C^{δ_1}	4.5
LEU284	C^{δ_2}	4.3
LEU290	C^{δ_2}	5.7
VAL293	C^{β}	4.6
VAL293	C^{γ_1}	4.0
VAL293	C^{γ_2}	4.2
LEU299	C^{γ}	5.3
LEU299	C^{δ_1}	5.2
LEU299	C^{δ_2}	4.4
HOH48	O	5.6

Figure 4(a) and (b) show portions of HSQC spectra of uniformly ^{15}N labeled MBP in complex with β-cyclodextrin. The β-cyclodextrin complex was chosen instead of the unliganded protein because backbone resonance assignments have been reported.[37] Several peaks in the HSQC spectrum show small changes in ^{1}H and ^{15}N chemical shift upon addition of xenon. With the available resonance assignments, the residues whose resonances shift can be mapped onto the structure. The peaks shown in Figure 4(a) and (b) correspond to Gly16 and Leu262, both of which line the xenon-binding cavity seen in the crystal structure. The association constant of xenon can be estimated by measuring the changes in the HSQC spectrum as a function of xenon concentration in solution. The chemical shifts of both Gly16 and Leu262 are plotted in Figure 4(e); fits using a simple two site binding model yield association constants of $20 \pm 10\ M^{-1}$. This value is in rough agreement with the refined occupancy of xenon in the crystal structure at 8 atm of xenon, assuming a solubility of xenon in solution of 4.4 mM atm^{-1} overpressure.

A similar experiment was conducted with ^{15}N labeled MBP in complex with maltose (Figure 4(c) and (d)). From reported assignments for this conformation (L. E. Kay, personal communication), the peaks corresponding to Gly16 and Leu262 were identified. These resonances show almost no change upon addition of xenon, indicating a lower

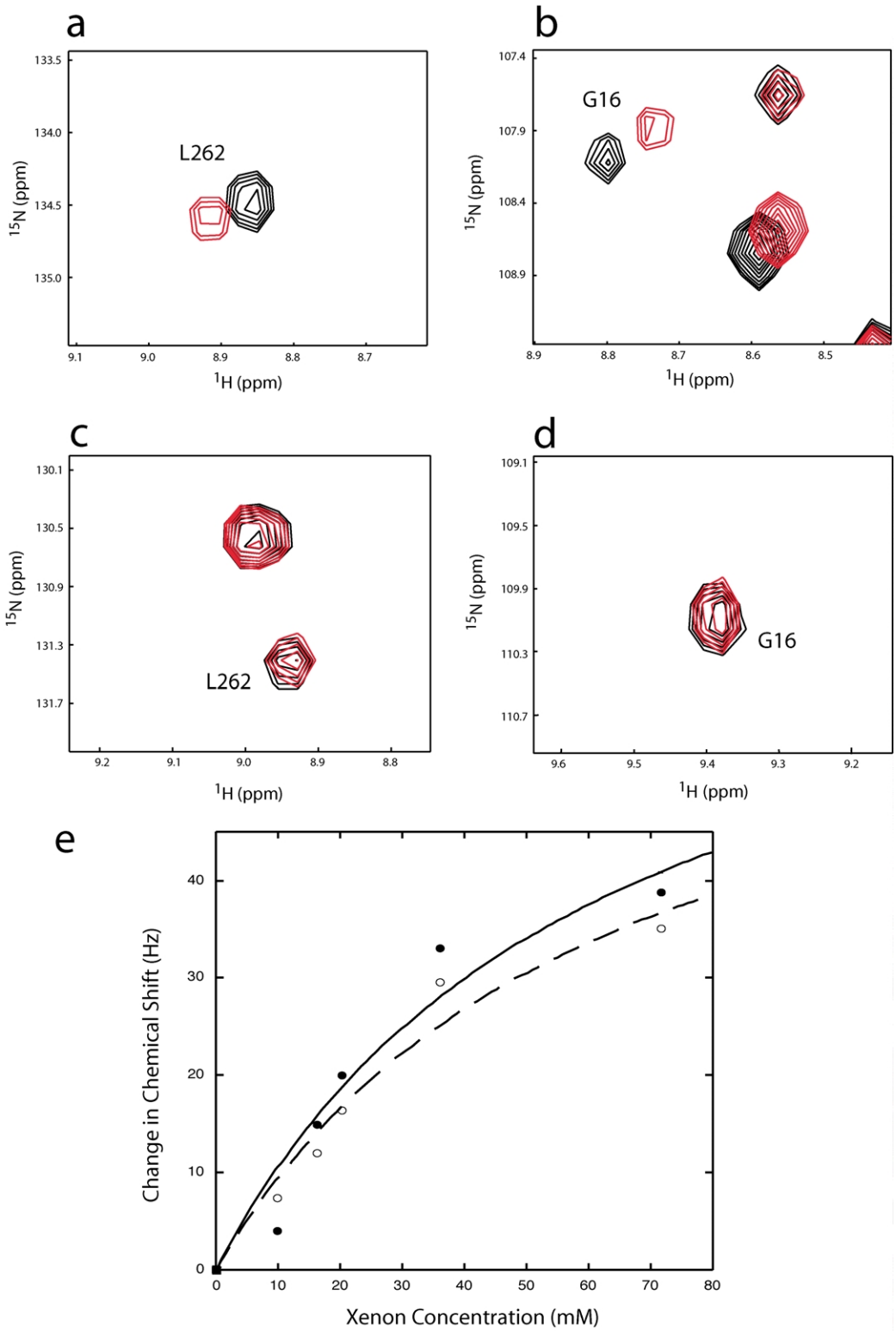

Figure 4. Evidence for a difference in xenon-binding affinity between the β-cyclodextrin and maltose complexes of MBP. (a) and (b) Portions of the ^{1}H–^{15}N HSQC correlation spectra of 0.4 mM MBP in solution with 2 mM β-cyclodextrin and no xenon (black) and 72 mM xenon (red). The resonances that have previously been assigned to Leu262 and Gly16 shift with increasing xenon concentration; in the crystal structure, these resonances line the cavity where xenon is bound. (c) and (d) Portions of the ^{1}H–^{15}N HSQC correlation spectra of 0.4 mM MBP in solution with 2 mM maltose and no xenon (black) and 72 mM xenon (red). The lack of significant shift changes for the same resonances indicates a weaker affinity of xenon for the maltose complex at the binding site observed in the crystal structure. (e) Plots of the total change in chemical shift as a function of xenon concentration for the resonances shown in a (○) and b (●). Fits of the data to a two-site model yield an association constant of 20 ± 10 M^{-1} for xenon bound to the β-cyclodextrin complex.

Table 3. Xenon-binding sites in T4 lysozyme cavity mutants

Protein	PDB code	Site	Cavity volume (Å^3)	Xenon occupancy
Wild-type	1C6T	1	58[a]	0.6
L121A	1C65	1	165[a]	0.7
L99A	1C6K	1	115[b]	0.7
L99A	1C6K	2	47[b]	0.6

[a] Reported.[7]
[b] Calculated as described in Materials and Methods.

affinity of xenon for the maltose complex at the binding site identified in the crystal structure. Small shifts in other peaks, corresponding to residues away from this binding site, were observed upon addition of xenon in both spectra. These shifts suggest other weak binding sites with occupancies too low to observe in the crystal structure. Considering that the small changes in peak position were of the same magnitude for both complexes, it is likely that the change in conformation does not affect the affinity at these other sites, so they do not contribute significantly to the change in ^{129}Xe shift.

^{129}Xe chemical shifts of xenon in solution with T4 lysozyme cavity mutants

The observed ^{129}Xe chemical shift of xenon in protein solutions is determined by contributions from all specific and non-specific xenon–protein interactions. Our strategy for revealing the contribution of a particular interaction entails altering the accessibility of xenon to a single binding site while the rest of the interactions in solution remain constant. The crystal structures of wild-type T4 lysozyme (WT*), and the variants L99A and L121A with xenon bound to internal cavities have been reported.[7] Structures of L99A with benzene and *n*-butylbenzene bound in its cavity have also been determined.[38] Table 3 summarizes the volumes and xenon occupancies of these cavities in the structures.[7] We measured ^{129}Xe chemical shifts of xenon in solutions of these proteins. Figure 5(a) shows ^{129}Xe NMR spectra of 1.5 mM xenon in solution with WT* and L121A T4 lysozyme at a protein concentration of 0.3 mM; results of the protein titration are plotted in Figure 5(b). Because the proteins are identical except for the structure of the xenon-binding cavity, the change in α value between WT* ($\alpha = 2.3 \pm 0.9 \times$ ppm mM^{-1}) and L121A ($\alpha = 0.9 \pm 0.1$ ppm $\times$ mM^{-1}) can be attributed to different contributions to the overall shift from this site.

The structure of L99A at 8 atm xenon revealed two primary binding sites (numbered 1 and 2 in order of decreasing xenon occupancy) and a third with much lower xenon occupancy.[7] To simplify data analysis and discussion, we consider only the two primary sites with any effects of site 3 subsumed by site 1. This approximation should be good considering that the xenon affinity for site 3 is much lower and that contributions from all sites to the overall chemical shift are additive (see below). Structures of L99A in the presence of benzene and *n*-butylbenzene show that these organic ligands bind to the same interior cavity as xenon, with affinities measured by calorimetric analysis of 5.7×10^3 M^{-1} and 7.0×10^4 M^{-1}, respectively.[7,38] The structures indicate that binding of benzene should inhibit binding of xenon to site 1, and binding of *n*-butylbenzene should inhibit binding of xenon to both sites. Thus, comparison of ^{129}Xe chemical shifts for titrations with L99A in the absence and presence of these ligands can resolve the contributions to the observed shifts from each specific site.

^{129}Xe NMR spectra of 1.5 mM xenon in solution with 0.3 mM L99A alone and with benzene and *n*-butylbenzene are shown in Figure 6(a). The addition of benzene has a small effect, while addition of *n*-butylbenzene has a larger effect on both the shift and width of the xenon resonance. The significant decrease in peak width with *n*-butylbenzene indicates that the spin interaction and/or exchange contribution to spin–spin relaxation have been reduced. Full titrations are shown in Figure 6(b) for L99A. The modest change in slope between the titrations with ($\alpha = 2.4 \pm 0.1 \times$ ppm mM^{-1}) and without ($\alpha = 2.7 \pm 0.1$ ppm $\times$ mM^{-1}) benzene indicates that site 1 contributes only a small amount to the overall shift. The slope of the L99A + benzene titration ($\alpha = 2.4 \pm 0.1 \times$ ppm mM^{-1}) is similar to the slope of the wild-type titration ($\alpha = 2.3 \pm 0.1$ ppm mM^{-1}). The benzene insensitive site (site 2) is in the same cavity as the wild-type site, hence binding-induced shifts are expected to be similar. The α value for L99A is significantly less ($\alpha = 0.9 \pm 0.1$ ppm $\times$ mM^{-1}) in the presence of *n*-butylbenzene, indicating a significant contribution to the observed shift from site 2.

As discussed further below, determination of the absolute chemical shift of xenon bound to a cavity requires a separate measurement of the binding affinity. We have measured association constants of xenon with L99A in the absence and presence of benzene by monitoring changes of protein resonance chemical shifts with xenon concentration. Backbone and side-chain dynamics of L99A in the presence of xenon have previously been studied by heteronuclear NMR; however, xenon affinities were not reported.[39] Figure 7 shows portions of the HSQC spectra of a sample containing 1.2 mM ^{15}N labeled L99A with and without both xenon and benzene. Comparison of peak positions in the four spectra yields two patterns for changes in chemical shift upon addition of the ligands. Some resonances, exemplified by the peaks in Figure 7(a), show changes in chemical shift upon addition of benzene but have the same limiting shift upon titration of xenon. These peaks likely correspond to amide protons near site 1, which is the

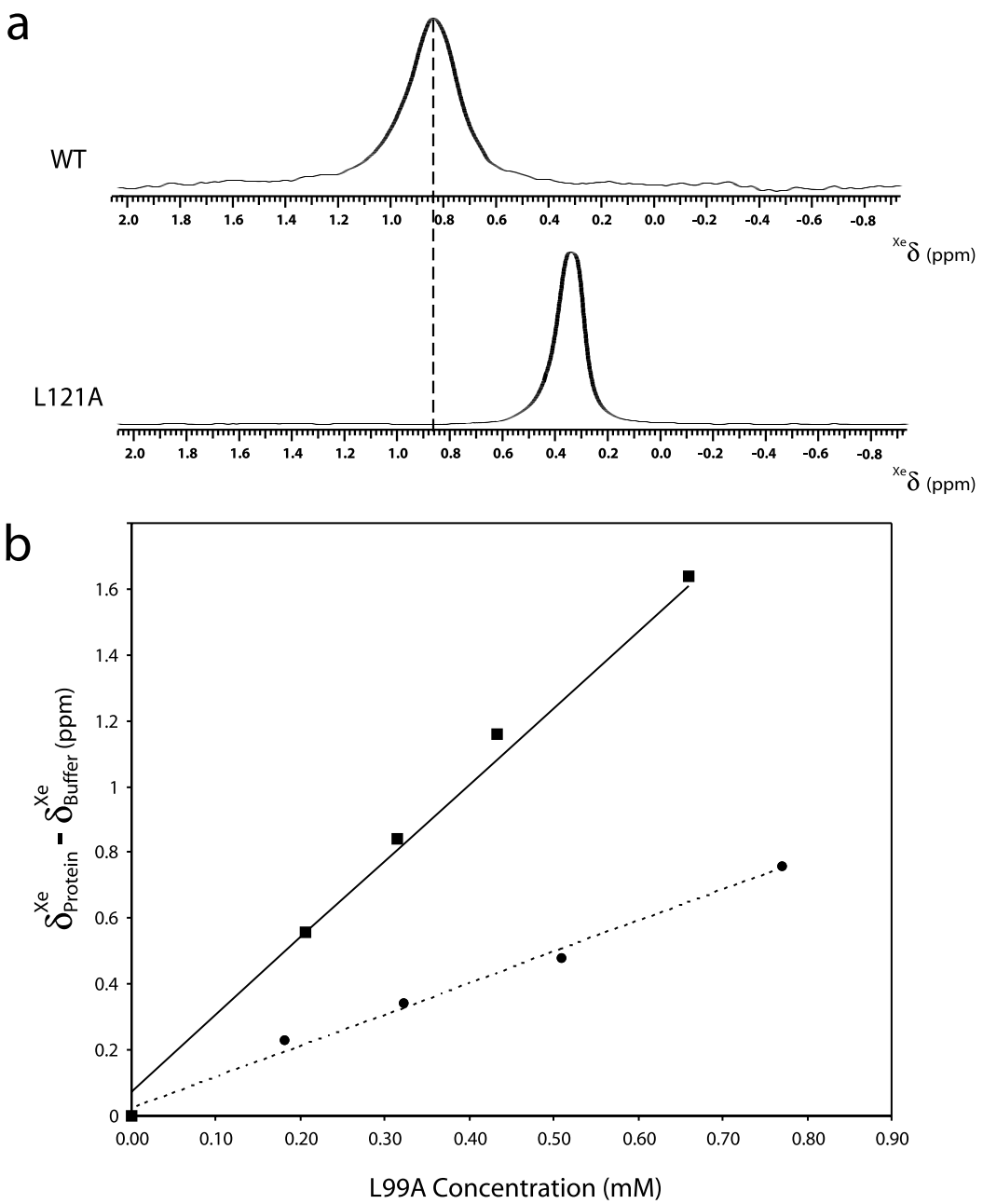

Figure 5. Effect of changing xenon-binding site structure on ^{129}Xe chemical shifts. (a) ^{129}Xe NMR spectra of 1.5 mM xenon in solution with 0.3 mM WT* and L121A T4 lysozyme. (b) Plot of the changes in ^{129}Xe chemical shift as a function of protein concentration for xenon in solution with WT* (■) and L121A (●). The difference in slope between the WT* titration ($\alpha = 2.3 \pm 0.1$ ppm mM^{-1}) and the L121A titration ($\alpha = 0.9 \pm 0.1$ ppm mM^{-1}) results from different contributions to the chemical shift from the xenon-binding site in each protein. The smaller WT* cavity induces a larger downfield shift than the larger L121A cavity.

benzene-binding site. The identical limiting shifts in the presence of xenon suggest that xenon can compete with benzene for the same binding site. However, comparison of affinity constants determined from these site 1 reporters in the absence and presence of benzene indicates that the affinity of xenon for site 1 is five times less with the amount of benzene present for ^{129}Xe NMR experiments. The titration curve without benzene for the site 1 reporter in Figure 7(a) is shown in Figure 7(c). Peaks following the second pattern (Figure 7(b)) show little or no change in chemical shift upon addition of benzene and have similar shifts in the presence and absence of benzene upon addition of saturating concentrations of xenon. In addition, the affinity of xenon deduced from these resonances does not change with addition of benzene. These peaks likely correspond to amide protons near site 2 in the protein, at some distance from the benzene-binding site. The relevant affinity

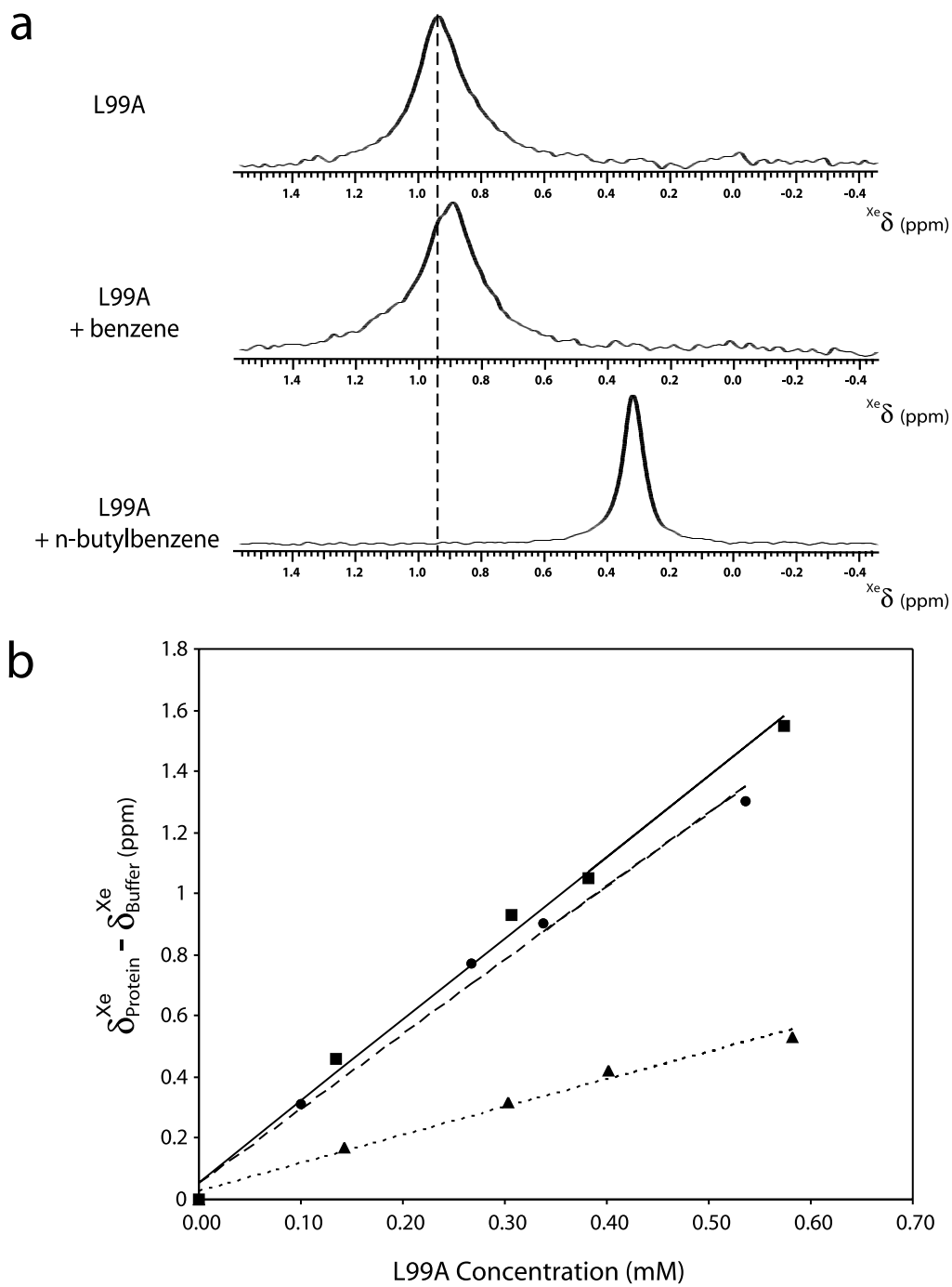

Figure 6. Effects of inhibiting xenon-binding sites on ^{129}Xe chemical shifts. (a) ^{129}Xe NMR spectra of 1.5 mM xenon in solution with 0.3 mM L99A T4 lysozyme and L99A with benzene and *n*-butylbenzene. (b) Plot of the changes in ^{129}Xe chemical shift as a function of protein concentration for xenon in solution with L99A alone (■) and L99A with benzene (●) and *n*-butylbenzene (▲). The difference in slope between the L99A titrations without ($\alpha = 2.7 \pm 0.1$ ppm mM^{-1}) and with benzene ($\alpha = 2.4 \pm 0.1$ ppm mM^{-1}) corresponds to the contribution from xenon–protein interactions at site 1, while the difference in slope between the benzene and *n*-butylbenzene ($\alpha = 0.9 \pm 0.1$ ppm mM^{-1}) titrations corresponds to the contribution from interactions at site 2.

constant for site 2 reporters is that measured in the presence of benzene, because the effect of inhibiting site 2 on the ^{129}Xe chemical shift was observed with benzene present. The titration curve in the presence of benzene for the site 2 reporter in Figure 7(b) is shown in Figure 7(c). A summary of the association constants measured from the two sets of reporters is given in Table 4. The reported values are the average of fits of chemical shift data from three reporters in each set; the reported error is the associated standard deviation for the three derived values.

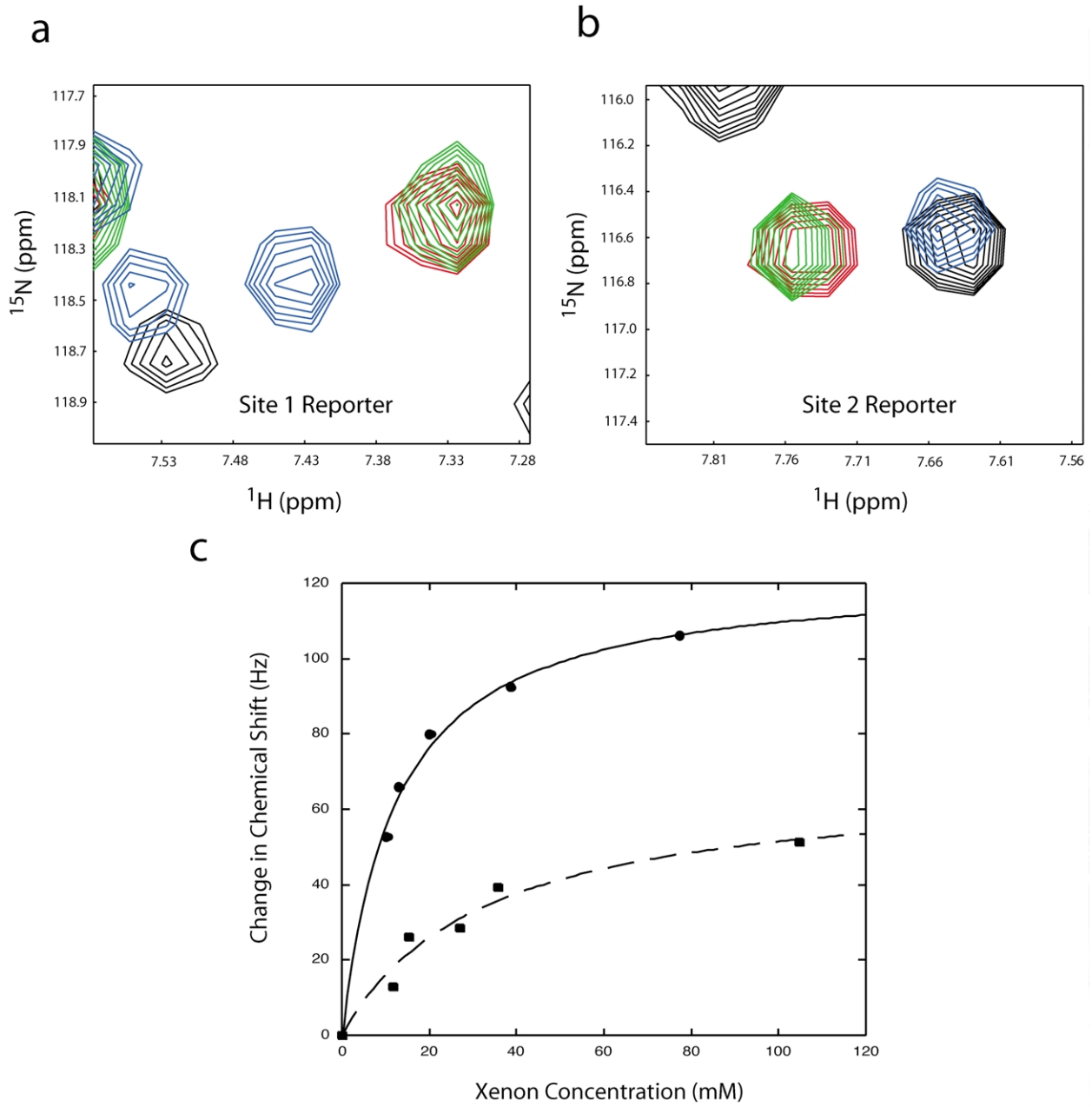

Figure 7. Determination of xenon–L99A binding affinities. (a) and (b) Portions of the ^{1}H–^{15}N HSQC correlation spectra of 1.2 mM L99A T4 lysozyme in solution alone (black), with benzene (blue), with 77 mM xenon (red), and with both benzene and 105 mM xenon (green). Resonances that show changes in chemical shift with addition of xenon correspond to protons near the xenon-binding sites. Peaks with significant chemical shift changes upon addition of benzene (a) correspond to amide protons near site 1, while resonances with small shifts (b) correspond to protons near site 2. (c) Plots of the total change in chemical shift as a function of xenon concentration for the resonances shown in (a) and (b). Fits of the data to a two-site model yield an association constant of 90 ± 10 M^{-1} for xenon bound to site 1 in the absence of benzene (●) and 30 ± 10 M^{-1} for xenon bound to site 2 in the presence of benzene (■).

Discussion

Detecting xenon-binding sites in proteins by ^{129}Xe chemical shift data

The changes in ^{129}Xe chemical shift with protein concentration can be described by a model that treats all specific and non-specific interactions as weak binding sites. In general, the observed shift (δ_{obs}), referenced to the shift in buffer, can be written as the average chemical shift of xenon in each site (δ_i) weighted by the occupancy:

$$\delta_{obs} = \sum_i \delta_i \frac{[Xe]_i}{[Xe]_{total}} = \sum_i \delta_i \frac{K_i([Xe]_{total} - [Xe]_i)([Protein]_{total} - [Xe]_i)}{[Xe]_{total}} \quad (1)$$

Table 4. Determination of ^{129}Xe chemical shifts of xenon bound to T4 lysozyme L99A

Cavity	Titration comparison	$\Delta\alpha = \delta_{site}K_{site}$ (ppm mM^{-1})	K_{site} (M^{-1})[a]	$\Delta\delta_{site}$ (ppm)[b]	δ^* (ppm)[c]
Site 1	L99A/L99A + benzene	0.3 ± 0.2	90 ± 40	3 ± 4	198 ± 4
Site 2	L99A + benzene/L99A + *n*-butylbenzene	1.5 ± 0.2	50 ± 10	30 ± 10	225 ± 10

[a] The reported affinity constant is the average constant determined from L99A HSQC data. For site 2, the affinity was determined in the presence of benzene.
[b] Chemical shift relative to the shift of xenon in buffer. Error is estimated from the relative errors in the measurements of $\Delta\alpha$ and K_{site}.
[c] Absolute chemical shift referenced to the shift of xenon gas in the limit of zero density.

where δ_i is also referenced to the shift in buffer and K_i is the association constant of xenon with each site. In the limit that a small amount of xenon is bound to each site, (i.e. $[Xe]_i \ll [Xe]_{total}$, $[Protein]_{total}$) the above equation reduces to:

$$\delta_{obs} = \sum_i \delta_i K_i [Protein]_{total} = \alpha [Protein]_{total} \quad (2)$$

where

$$\alpha = \sum_i \delta_i K_i$$

Thus, the slopes of protein titration data such as those shown in Figures 1, 5, and 6 are indicative of the affinity and effect on the shift of all xenon–protein interactions in solution. Due to the small values of K_i and the low total xenon and protein concentrations typically used, these titrations are indeed conducted in the limit in which a small fraction of xenon is bound. As seen in equation (2) and the data in Figure 1, in this limit the observed slope α is independent of the xenon concentration in solution.

Considering that the contributions to α from non-specific interactions scale roughly with protein accessible surface area,[28] deviations from anticipated values of α suggest the presence of specific binding interactions. In particular, it appears that proteins with $\alpha_{native} > \alpha_{denatured}$ must contain a site that interacts more strongly with xenon than average surface sites because the surface area (and hence the number of non-specific interactions) increases upon denaturation. The crystal structure of MBP with xenon reported here confirms the presence of the binding site predicted by comparison of the α values in Figure 1. NMR and crystallographic data on other proteins confirm that proteins with $\alpha_{native} > \alpha_{denatured}$ bind xenon specifically; examples include the T4 lysozymes studied here, myoglobin,[26,40] and bovine serum albumin.[21,28] We note that in cases for which $\alpha_{native} < \alpha_{denatured}$ xenon binding cannot be precluded as the possibility exists for a specific site with a limiting shift that is upfield from the shift of xenon in buffer (i.e. $\delta_i < 0$ in equation (2)). Xenon binding in such cases may be confirmed by observing widths of ^{129}Xe resonances. Although non-specific interactions result in some line broadening,[28] the effects of specific interactions are more pronounced and can likely be distinguished.

^{129}Xe shifts in protein cavities can be determined in the limit of weak binding and correlate with cavity size

The sensitivity of the ^{129}Xe shift to its local environment has been exploited in studies of xenon interacting with materials such as zeolites, clathrates, and nanotubes.[41–43] Xenon can probe cavities in these structures, reporting on properties such as size, shape, chemical composition, and occupancy of the gas. Complementary information from crystallographic and ^{129}Xe NMR experiments has enabled interpretation of observations with hydrophobic cavities in proteins. The low affinity of xenon for cavities makes determination of the limiting shift of bound xenon (δ_{site}) difficult. Fast exchange of xenon among all environments in solution prevents direct observation of δ_{site} from a ^{129}Xe NMR spectrum. The limiting shift of xenon bound to myoglobin has been estimated from titrations in which a significant fraction of xenon is bound.[26,27] However, this method is not ideal as it requires the addition of large amounts of protein to solution and the determination of shifts from broad spectral lines, nor it is general as xenon–protein interactions are typically too weak to attain substantial occupancy.

We demonstrate here that δ_{site} can be determined even when a small fraction of xenon is bound by comparing titrations in which the interaction is available and blocked. As seen in equation (2), each contribution to the concentration-normalized shift or α value of a protein depends on both δ_{site} and the affinity (K_{site}); thus, an independent measurement of the binding constant allows calculation of δ_{site}. For example, the difference in α values between the L99A and L99A + benzene titrations marks the contribution from site 1 in the protein (i.e. from equation (2), $\Delta\alpha = \delta_{site\ 1}K_{site\ 1}$). Using the association constant ($K_{site\ 1} = 90 \pm 40\ M^{-1}$) obtained from the HSQC titration (Figure 7), the ^{129}Xe chemical shift of xenon bound to the cavity relative to the shift in buffer ($\delta_{site\ 1} = 3 \pm 4$ ppm) and the absolute shift referenced to xenon gas in the limit of zero density ($\delta* = 198 \pm 4$ppm) can be estimated. Table 4 gives the limiting shift derived for xenon bound to each cavity in L99A.

Comparison of the α values of wild-type and cavity mutants of T4 lysozyme reveals that smaller cavities give rise to larger downfield ^{129}Xe shifts

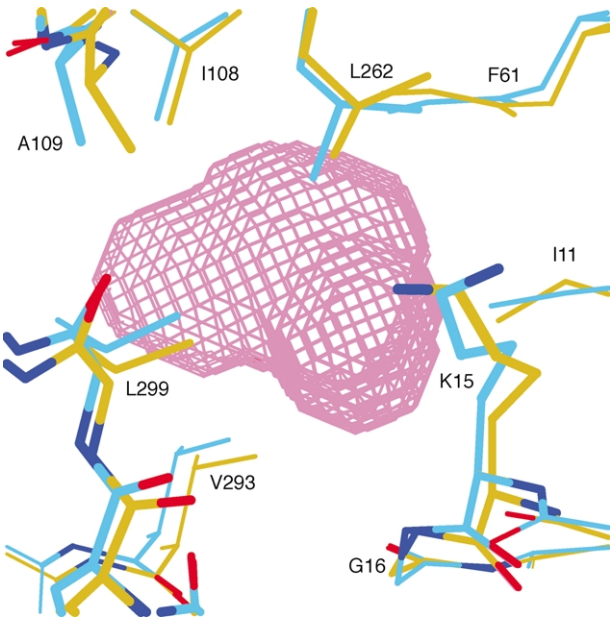

Figure 8. Comparison of the structure of the xenon-binding cavity in MBP in the β-cyclodextrin (brown) and maltose (cyan) complexes. The cavity space in the β-cyclodextrin structure is shown in magenta. The position of most of the residues that line the cavity is similar except for Lys15, which moves to hydrogen bond to the reducing glycosyl unit of maltose. This subtle change in the cavity likely accounts for the sensitivity of the ^{129}Xe chemical shift to the conformation of MBP.

than those from larger cavities. Replacing Leu121 in T4 lysozyme with alanine enlarges the xenon-binding cavity from 58 Å^3 to 165 Å^3; this change in structure induces a change in α values from 2.3 ppm mM^{-1} to 0.9 ppm mM^{-1} as seen in Figure 5. While contributions from non-specific interactions remain the same, the contribution to α from this specific interaction at the cavity is greater in the wild-type protein (i.e. $\delta_{WT^*}K_{WT^*} > \delta_{L121A}K_{L121A}$). The refined occupancy of xenon in each cavity is 0.7 for crystals of each protein at 8 bar of xenon.[7] Assuming that the same crystallographic occupancies indicate similar affinities in solution ($K_{WT^*} \sim K_{L121A}$), the ^{129}Xe shift of xenon bound to the smaller cavity of the wild-type protein must be further downfield than xenon bound to L121A ($\delta_{WT^*} > \delta_{L121A}$). Titration data for L99A indicate that xenon interactions with the smaller site 2 cavity (47 Å^3) result in a larger downfield contribution to the α value than interactions with the larger site 1 cavity (115 Å^3). The similar affinities determined from the HSQC data indicate that these different contributions are due to different values of the limiting shift of bound xenon (i.e. $\delta_{site\ 2} = 30 \pm 10$ ppm $> \delta_{site\ 1} = 3(\pm 4)$ ppm). The observation that smaller cavities in proteins induce larger downfield ^{129}Xe shifts is consistent with studies of xenon in water clathrates and zeolites.[41,42]

Change in structure of the xenon-binding site correlates with the sensitivity of the ^{129}Xe chemical shift to MBP conformation

Addition of maltose to native MBP induced an almost twofold change in the α value.[25] The sensitivity of the ^{129}Xe shift to native state conformation suggests the possibility of using xenon to detect protein functional states or ligand binding events. Understanding the structural basis for the change in chemical shift with conformation is necessary to extend such an assay to other biomolecular systems. The twofold difference in α between the protein states is too large to result from a change in the chemical composition or accessibility of the protein surface. Rather, we proposed that the difference resulted from altered interactions at a specific xenon-binding site.[25] The crystal structure of unliganded MBP with xenon confirms the presence of such a binding site. Because MBP-induced ^{129}Xe shifts depend on the bound shift and the binding constant, a change in either parameter upon binding maltose would explain the change in α values. The xenon titration followed in the HSQC spectra (Figure 4) indicates that the affinity of xenon for MBP is greater in the open conformation than the closed conformation; this difference in affinity is likely due to a change in the structure of the xenon-binding cavity that occurs when MBP binds maltose, but not β-cyclodextrin.

Figure 8 shows the xenon-binding cavity in the published structures of MBP complexed with β-cyclodextrin (PDB code: 1DMB) and maltose (PDB code: 1ANF).[35,44] The two structures were superimposed by minimizing C^α distances between residues in the N-terminal domain (5–109, 284–319). The cavity space found by VOIDOO in the β-cyclodextrin structure is shown in magenta.[45] Comparison of the structures reveals only small changes in the positions of the residues that line the cavity. This similarity in cavity structure is not surprising considering that the cavity is located entirely within the N-terminal domain and that the overall conformation of the two complexes differs by a rigid body hinge bend of the two domains. The difference in the position of Lys15 between the two structures, however, is prominent and results from the fact that the side-chain amino group hydrogen bonds specifically to maltose in the nearby sugar-binding cleft. This hydrogen bonding reduces the flexibility of the lysine, as seen in the lower refined *B*-factors for the side-chain atoms in the maltose structure (~10–20 Å^2) relative to the unliganded and β-cyclodextrin structures (~20–30 Å^2). The change in lysine position results in a modest difference in calculated cavity volumes between the maltose-bound structure (75 Å^3) and the unliganded (95 Å^3) and β-cyclodextrin (93 Å^3) structures. It remains unclear whether this change in cavity volume is the cause of the lower affinity of xenon for the maltose complex, particularly considering that xenon localizes in the cavity away from the

position of the lysine. However, the correlations between the ^{129}Xe chemical shift data, xenon–protein affinity, and the hydrogen bonding of the lysine strongly suggest that this residue plays a role in the mechanism for detection of the conformational change by ^{129}Xe NMR.

Applications of ^{129}Xe NMR in biochemical assays

The results presented here demonstrate the sensitivity of the ^{129}Xe chemical shift to binding affinity and binding-site structure. The ability to correlate these properties with their effects on chemical shift may lead to a number of applications of ^{129}Xe NMR in biochemical and structural studies of proteins. For example, specific xenon–protein interactions can be identified from ^{129}Xe chemical shift data alone. This simple assay for xenon binding may be of interest to X-ray crystallographers interested in using xenon to generate heavy atom derivatives; good candidates are proteins with $\alpha_{native} > \alpha_{denatured}$. Because $\alpha_{denatured}$ scales roughly with protein size, it may only be necessary to measure α_{native} in order to conclude that a protein binds xenon. Although the use of laser-polarized ^{129}Xe facilitates shift measurements by increasing the signal-to-noise ratio, protein titrations can be done with natural ^{129}Xe polarization and take only a few hours with standard NMR spectrometers.

The sensitivity of the ^{129}Xe chemical shift to MBP conformation and interactions indicates that ^{129}Xe NMR can be used as a detector of ligand-binding events and protein conformation in solution. The advantages of ^{129}Xe NMR are that reporting is done by a chemically inert, external species in solution, alleviating the need for labeling molecules of interest with radioisotope or fluorescent probes, and biomolecular samples can be recovered in their native state. In addition, ^{129}Xe spectra are simple with no background, making them sensitive and easy to analyze. The MBP structure with bound xenon suggests that the maltose-induced change in ^{129}Xe shift results from the presence of a natural, specific xenon-binding site that undergoes a change in structure upon ligand binding. We are currently investigating whether such an effect can be induced by creating xenon-binding sites in regions of proteins that have structural differences among conformers.

Materials and Methods

Protein expression and purification

MBP from *Escherichia coli* was expressed and purified as described.[25] Wild-type and mutant T4 lysozymes, all cystein free variants, were expressed as described,[29] except L99A, which was subcloned into a pET vector (Novagen) and expressed in the *E. coli* strain BL21(DE3). ^{15}N labeled MBP and T4 lysozyme were isolated from *E. coli* grown in M9 media with $^{15}NH_4Cl$ as the only nitrogen source. All T4 lysozymes were purified using CM ion exchange resin (Pharmacia Biotech) in a 50 mM Tris buffer at pH 7.4. All purified proteins were dialyzed against water for three days, with a change of water twice a day prior to lyophilization.

^{129}Xe NMR data collection

Lyophilized protein samples were dissolved in 1 ml of buffer containing 100 mM Tris (pH 7.6 for MBP, pH 7.4 for the T4 lysozymes) and 20% ^2H_2O. For the MBP titration under denaturing conditions, the buffer consisted of 100 mM citric acid (pH 3.0), 6 M urea, and 20% ^2H_2O. The protein stock solution was diluted with buffer to make four 400 μl samples at different concentrations; a fifth sample of 400 μl of buffer alone was used as a reference. Each sample in the L99A T4 lysozyme titrations done in the presence of organic molecules was prepared by addition of 0.5 μl of the neat organic ligand to the 400 μl of protein solution. Previous studies demonstrated that this preparation maintains sufficient ligand in solution to saturate the binding sites over the course of a short experiment such as ^{129}Xe NMR data collection.[46] We have found that inconsistencies in the buffer composition of samples being compared can affect ^{129}Xe NMR chemical shifts. For this reason, many precautions were taken to ensure that the ionic strength, pH, and ^2H_2O composition of the protein stock solution and buffer used for subsequent dilutions were kept the same. The use of KOH, HCl, and KCl to make any necessary adjustments is convenient because K^+ and Cl^- have similar effects on the ^{129}Xe chemical shift.[47]

A portion of the buffer (5–10 ml) was added to a glass bulb for mixing of laser-polarized xenon as previously described.[21] The bulb has an inlet that can be opened *via* a Teflon valve to a vacuum or the source of laser-polarized xenon and has a septum covered outlet, through which buffer can be withdrawn with a syringe. The buffer was degassed using three freeze–pump–thaw cycles prior to the introduction of laser-polarized gas in order to remove oxygen, which could relax the xenon. Natural abundance ^{129}Xe (Isotech) was polarized with standard procedures. A pressure gauge was used to monitor the amount of gas transferred from the polarization apparatus to the bulb. The xenon concentration in the buffer is assumed to be linear with gas overpressure with a solubility of 4.4 mM atm^{-1}.[48] After vigorous shaking, 200 μl of buffer was withdrawn from the bulb and mixed rapidly with a protein sample in a standard 5 mM NMR tube. ^{129}Xe NMR spectra were acquired immediately following mixing for each of the five samples. Spectra were acquired at room temperature on a 300 MHz (proton frequency) Varian Inova spectrometer. The denatured MBP titration was done using unpolarized xenon as previously described for other denatured proteins.[28] Following NMR data collection, protein sample concentrations were determined by absorbance at 280 nm ($\varepsilon_{280} = 66,350\ M^{-1}\ cm^{-1}$ for MBP and $\varepsilon_{280} = 25,440\ M^{-1}\ cm^{-1}$ for T4 lysozyme). Reported ^{129}Xe shifts are referenced to that of xenon in buffer alone; the chemical shift of xenon in buffer (except that containing 6 M urea), referenced to the shift of xenon gas in the limit of zero density, was typically ≈195 ppm.

Xenon affinity determination

^{1}H–^{15}N HSQC correlation spectra were acquired with uniformly ^{15}N labeled MBP and T4 lysozyme L99A.

MBP samples (0.4 mM) were prepared in buffer containing 20 mM sodium phosphate (pH 7.2), 100 μM EDTA, 10% ^2H_2O and 2 mM of either β-cyclodextrin or maltose. T4 lysozyme samples (1.2 mM) were prepared in buffer containing 50 mM sodium phosphate (pH 5.8), 25 mM NaCl, 10% ^2H_2O and 0.5 μl benzene where indicated. The presence of benzene was confirmed during the titration by observing its effect on the protein spectrum in the absence of xenon. Samples were in medium wall NMR tubes adapted with a screw-cap to allow xenon over pressures of several atmospheres. Samples were frozen and degassed once prior to addition of xenon, and pressures were measured with a gauge upon recovery of the gas after data acquisition. NMR spectra were acquired with 600 MHz and 500 MHz Bruker DRX spectrometers and processed using the NMRPipe and NMRView software packages.[49,50] Titration data were fit to a two site binding model using Kaleidagraph; reported errors in association constants correspond to either fitting errors or, in cases where chemical shift changes from a number of different resonances were averaged, standard deviations of a distribution.

Cavity volume calculations

Cavity volumes were calculated using VOIDOO.[45] We found that calculated volumes were often sensitive to the parameter values chosen for the grid size and probe radius parameters. In general, cavity searches with VOIDOO yielded no cavities when the van der Waals radius of xenon (2.2 Å) was used for the probe size. For calculations of cavities in T4 lysozyme L99A, grid (0.5 Å) and probe (radius = 1.4 Å) parameters were chosen such that a sample calculation of the volume of the WT* cavity was consistent with that reported.[7] Calculations of the cavity volumes of site 1 and site 2 in L99A were done by removing the xenon atom within the cavity under consideration from the PDB coordinate file. For consistency, cavities in MBP were calculated using similar parameters, except a probe radius of 1.45 Å was needed to close the cavity from the grid beyond the protein surface.

Crystal structure determination

Crystallization of unliganded MBP was done under similar conditions to those reported.[31] Crystals were obtained at room temperature using the hanging-drop vapor-diffusion method. 2 μl protein solution (16 mg ml^{-1}) was mixed with an equal volume of well solution containing 10 mM sodium citrate and 23% (w/v) PEG 8000 (pH 6.6). Crystals with a size of 0.2 mm × 0.05 mm × 0.05 mm appeared in two days. Well solution with 10% (v/v) glycerol was used as a cryoprotectant. Partial data sets collected for these crystals in the absence of xenon showed they were isomorphous with crystals used to solve reported structures (data not shown).[30,31] Crystals were pressurized with xenon gas at 8 atm for 15 minutes and 12 atm for 30 minutes using a commercially available chamber (Hampton Research) prior to freezing in liquid nitrogen. Pressures were chosen on the basis of the calculated affinity in solution from the NMR data. For an exposure time of 15 minutes at 8 atm, crystal diffracted in space group $P1$ with dimensions $a = 38.2$ Å, $b = 44.0$ Å, $c = 57.6$ Å, $\alpha = 100.7°$, $\beta = 101.4°$, $\gamma = 102.6°$. For an exposure time of 30 minutes at 12 atm, crystals lost isomorphism (space group $P1$, cell dimensions $a = 52.2$ Å, $b = 58.3$ Å, $c = 64.9$ Å, $\alpha = 89.3°$, $\beta = 82.4°$, $\gamma = 71.8°$) and had higher mosaicity. The adverse effects of the longer exposure time have been reported elsewhere and are likely a result of crystal drying despite saturation of the chamber with vapor from the mother liquor.[4]

The diffraction data were collected at the Advanced Light Source (Berkeley, CA) using the 5.0.3 and 8.3.1 beam lines using an ADSC detector and a wavelength of 1.0 Å. A crystal-detector distance of 220 mm was used to collect data to a diffraction of 1.8 Å (92.3% completion). The isomorphous data set (xenon exposure time 15 minutes at 8 atm) was integrated and scaled to 1.8 Å (92.3% completion) with MOSFLM[51] and the CCP4 suite[52] using the Elves interface (J. M. Holton, unpublished results). Unambiguous identification of electron density corresponding to xenon was made by generating a difference-Fourier map using structure factors from the unliganded structure in the Protein Data Bank (PDB code 1OMP). The map was generated by treating 1OMP as a native data set and our diffraction data set as a derivative. Structure refinement was done using CNS 1.0,[53] beginning with 1OMP as an initial model. Initial refinement consisted of rounds of rigid-body, simulated annealing, and B-group refinement. After the R-factor and R_{free} reached 25% and 27%, respectively, water and xenon were added to the model, followed by subsequent rounds of energy minimization, B-individual, and manual refinement. After the R-factor and R_{free} reached 21% and 23%, occupancy of xenon was determined using a combination of occupancy and B-individual refinement. The process of occupancy refinement was repeated with a number of different initial xenon B-factors; the final refined occupancy always fell within the range of 0.45–0.54. Data collection and refinement statistics are listed in Table 1. Manual refinement and graphics visualization were done with the O software package.[54] Geometry parameters were monitored using PROCHECK.[55]

Accession code

Coordinates and structure factors for the unliganded MBP crystal structure with xenon have been deposited in the Protein Data Bank under accession code 1LLS.

Acknowledgements

The authors acknowledge Professor B. Matthews for providing T4 lysozyme expression vectors, T. Lawhead for his expert glassblowing and advice, and Professors C. J. Jameson, S. Mowbray, and L. E. Kay for helpful discussion. S.M.R. acknowledges the National Science Foundation and E.J.R. acknowledges Lucent Technologies/Bell Laboratories for predoctoral fellowships. This work was supported by the Director, Office of Energy Research, Office of Basic Energy Sciences, Physical Biosciences and Material Sciences Divisions, of the US Department of Energy under Contract No. DE-AC03-76SF00098 and through the Office of Naval Research (MDI-II).

References

1. Schoenborn, B. C., Watson, H. C. & Kendrew, J. C. (1965). Binding of xenon to sperm whale myoglobin. *Nature*, **207**, 28–30.
2. Montet, Y., Amara, P., Volbeda, A., Vernede, X., Hatchikian, E. C., Field, M. J. *et al.* (1997). Gas access to the active site of Ni–Fe hydrogenases probed by X-ray crystallography and molecular dynamics. *Nature Struct. Biol.* **4**, 523–526.
3. Wentworth, P., Jr, Jones, L. H., Wentworth, A. D., Zhu, X., Larsen, N. A., Wilson, I. A. *et al.* (2001). Antibody catalysis of the oxidation of water. *Science*, **293**, 1806–1811.
4. Whittington, D. A., Rosenzweig, A. C., Frederick, C. A. & Lippard, S. J. (2001). Xenon and halogenated alkanes track putative substrate binding cavities in the soluble methane monooxygenase hydroxylase. *Biochemistry*, **40**, 3476–3482.
5. Tilton, R. F., Singh, U. C., Weiner, S. J., Connolly, M. I., Kuntz, I. D., Kollman, P. A. *et al.* (1986). Computational studies of the interaction of myoglobin and xenon. *J. Mol. Biol.* **192**, 443–456.
6. Mann, G. & Hermans, J. (2000). Modeling protein–small molecule interactions: structure and thermodynamics of noble gases binding in a cavity in mutant phage T4 lysozyme L99A. *J. Mol. Biol.* **302**, 979–989.
7. Quillin, M. L., Breyer, W. A., Griswold, I. J. & Matthews, B. W. (2000). Size *versus* polarizability in protein-ligand interactions: binding of noble gases within engineered cavities in phage T4 lysozyme. *J. Mol. Biol.* **302**, 955–977.
8. Anderson, M., Xu, Y. & Grissom, C. B. (2001). Electron spin catalysis by xenon in an enzyme. *J. Am. Chem. Soc.* **123**, 6720–6721.
9. Schiltz, M., Prangé, T. & Fourme, R. (1994). On the preparation and X-ray data collection of isomorphous derivatives. *J. Appl. Crystallog.* **27**, 950–960.
10. Soltis, S. M., Stowell, M. H. B., Wiener, M. C., Phillips, G. N., Jr & Rees, D. C. (1997). Successfull flash-cooling of xenon-derivatized myoglobin crystals. *J. Appl. Crystallog.* **30**, 190–194.
11. Ogata, C. M. (1998). MAD phasing grows up. *Nature Struct. Biol.* **5**, 638–640.
12. Owen, D. J. & Evans, P. R. (1998). A structural explanation for the recognition of tyrosine-based endocytotic signals. *Science*, **282**, 1327–1332.
13. Hamburger, Z. A., Brown, M. S., Isberg, R. R. & Bjorkman, P. J. (1999). Crystal structure of invasin: a bacterial integrin-binding protein. *Science*, **286**, 291–295.
14. Ratcliffe, C. (1998). Xenon NMR. *Annu. Rep. NMR Spectrosc.* **36**, 124–208.
15. Miller, K. W., Reo, N. V., Schoot Uiterkamp, A. J., Stengle, D. P., Stengle, T. R. & Williamson, K. L. (1981). Xenon NMR: chemical shifts of a general anesthetic in common solvents, proteins, and membranes. *Proc. Natl Acad. Sci. USA*, **78**, 4946–4949.
16. Tilton, R. F., Jr & Kuntz, I. D., Jr (1982). Nuclear magnetic resonance studies of xenon-129 with myoglobin and hemoglobin. *Biochemistry*, **21**, 6850–6857.
17. McKim, S. & Hinton, J. F. (1994). Evidence of xenon transport through the gramicidin channel: a 129-Xe NMR study. *Biochim. Biophys. Acta*, **1193**, 186–198.
18. Raftery, D., Long, H., Meersman, T., Grandinetti, P. J., Reven, L. & Pines, A. (1991). High field NMR of adsorbed xenon polarized by laser pumping. *Phys. Rev. Letters*, **66**, 584–586.
19. Walker, T. G. & Happer, W. (1997). Spin-exchange optical pumping of noble-gas nuclei. *Rev. Mod. Phys.* **69**, 629–642.
20. Bowers, C. R., Storhaug, V., Webster, C. E., Bharatam, J., Cottone, A., Gianna, R. *et al.* (1999). Exploring surfaces and cavities in lipoxygenase and other proteins by hyperpolarized xenon-129 NMR. *J. Am. Chem. Soc.* **121**, 9370–9377.
21. Wolber, J., Cherubini, A., Dzik-Jurasz, A. S., Leach, M. O. & Bifone, A. (1999). Spin–lattice relaxation of laser-polarized xenon in human blood. *Proc. Natl Acad. Sci. USA*, **96**, 3664–3669.
22. Landon, C., Berthault, P., Vovelle, F. & Desvaux, H. (2001). Magnetization transfer from laser-polarized xenon to protons in the hydrophobic cavity of the wheat nonspecific lipid tranfer protein. *Protein Sci.* **10**, 762–770.
23. Navon, G., Song, Y. Q., Room, T., Appelt, S., Taylor, R. E. & Pines, A. (1996). Enhancement of solution NMR and MRI with laser-polarized xenon. *Science*, **271**, 1848–1851.
24. Spence, M. M., Rubin, S. M., Dimitrov, I. E., Ruiz, E. J., Wemmer, D. E., Pines, A. *et al.* (2001). Functionalized xenon as a biosensor. *Proc. Natl Acad. Sci. USA*, **98**, 10654–10657.
25. Rubin, S. M., Spence, M. M., Dimitrov, I. E., Ruiz, E. J., Pines, A. & Wemmer, D. E. (2001). Detection of a conformational change in maltose binding protein by ^{129}Xe NMR spectroscopy. *J. Am. Chem. Soc.* **123**, 8616–8617.
26. Rubin, S. M., Spence, M. M., Goodson, B. M., Wemmer, D. E. & Pines, A. (2000). Evidence of nonspecific surface interactions between laser-polarized xenon and myoglobin in solution. *Proc. Natl Acad. Sci. USA*, **97**, 9472–9475.
27. Locci, E., Dehouck, Y., Casu, M., Saba, G., Lai, A., Luhmer, M. *et al.* (2001). Probing proteins in solution by ^{129}Xe NMR spectroscopy. *J. Magn. Reson.* **150**, 167–174.
28. Rubin, S. M., Spence, M. M., Pines, A. & Wemmer, D. E. (2001). Characterization of the effects of nonspecific xenon–protein interactions on ^{129}Xe chemical shifts in aqueous solution: further development of xenon as a biomolecular probe. *J. Magn. Reson.* **152**, 79–86.
29. Eriksson, A. E., Baase, W. A., Zhang, X.-J., Heinz, D. W., Blaber, M., Baldwin, E. P. & Matthews, B. W. (1992). Response of a protein structure to cavity-creating mutations and its relation to the hydrophobic effect. *Science*, **255**, 178–183.
30. Sharff, A. J., Rodseth, L. E., Spurlino, J. C. & Quiocho, F. A. (1992). Crystallographic evidence of a large ligand-induced hinge-twist motion between the two domains of the maltodexrin binding protein involved in active transport and chemotaxis. *Biochemistry*, **31**, 10657–10663.
31. Shilton, B. H., Shuman, H. A. & Mowbray, S. L. (1996). Crystal structures and solution conformations of a dominant-negative mutant of *Escherichia coli* maltose-binding protein. *J. Mol. Biol.* **2**, 364–376.
32. Prangé, T., Schiltz, M., Pernot, L., Colloc'h, N., Longhi, S., Bourget, W. & Fourme, R. (1998). Exploring hydrophobic sites in proteins with xenon and krypton. *Protines: Struct. Funct. Genet.* **30**, 61–73.
33. Spurlino, J. C., Lu, G.-Y. & Quiocho, F. A. (1991). The 2.3 Å resolution structure of the maltose- or maltodextrin-binding protein, a primary receptor of

bacterial active transport and chemotaxis. *J. Biol. Chem.* **266**, 5202–5219.
34. Stowell, M. H. B., Soltis, S. M., Kisker, C., Peters, J. W., Schindelin, H., Rees, D. C. *et al.* (1996). A simple device for studying macromolecular crystals under moderate gas pressures (0.1–10 MPa). *J. Appl. Crystallog.* **29**, 608–613.
35. Sharff, A. J., Rodseth, L. E. & Quiocho, F. A. (1993). Refined 1.8 Å structure reveals the mode of binding of β-cyclodextrin to the maltodextrin binding protein. *Biochemistry*, **32**, 10553–10559.
36. Kay, L. E. (2001). Nuclear magnetic resonance methods for high molecular weight proteins: a study involving a complex of maltose binding protein and beta-cyclodextrin. *Methods Enzymol.* **339**, 174–203.
37. Gardner, K. H., Zhang, X., Gehring, K. & Kay, L. E. (1998). Solution NMR studies of a 42 kDa *Escherichia coli* maltose binding protein/β-cyclodextrin complex: chemical shift assignments and analysis. *J. Am. Chem. Soc.* **120**, 11738–11748.
38. Morton, A. & Matthews, B. W. (1995). Specificity of ligand binding in a buried nonpolar cavity of T4 lysozyme: linkage of dynamics and structural plasticity. *Biochemistry*, **34**, 8576–8588.
39. Mulder, F. A. A., Hon, B., Muhandiram, D. J., Dahlquist, F. W. & Kay, L. E. (2000). Flexibility and ligand exchange in a buried cavity mutant of T4 lysozyme studied by multinuclear NMR. *Biochemistry*, **39**, 12614–12622.
40. Tilton, R. F., Jr, Kuntz, I. D., Jr & Petsko, G. A. (1984). Cavities in proteins: structure of a metmyoglobin–xenon complex solved to 1.9 Å. *Biochemistry*, **23**, 2849–2857.
41. Ripmeester, J. A., Ratcliffe, C. I. & Tse, J. S. (1988). The nuclear magnetic resonance of Xe-129 trapped in clathrates and some other solids. *J. Chem. Soc., Faraday Trans.* **84**, 3731–3745.
42. Bonardet, J., Fraissard, J., Gédéon, A. & Springuel-Huet, M. (1999). Nuclear magnetic resonance of physisorbed 129-Xe used as a probe to investigate porous solids. *Catal. Rev.: Sci. Eng.* **41**, 115–225.
43. Sozzani, P., Comotti, A., Simonutti, R., Meersmann, T., Logan, J. W. & Pines, A. (2000). A porous crystalline molecular solid explored by hyperpolarized xenon. *Angew. Chem. Int. Ed.* **39**, 2695–2698.
44. Quiocho, F. A., Spurlino, J. C. & Rodseth, L. E. (1997). Extensive features of tight oligosaccharide binding revealed in high-resolution structures of the maltodextrin transport/chemosensory receptor. *Structure*, **5**, 997–1015.
45. Kleywegt, G. J. & Jones, T. A. (1994). Detection, delineation, measurement, and display of cavities in macromoleclar structures. *Acta Crystallog. sect. D*, **50**, 178–185.
46. Morton, A., Baase, W. A. & Matthews, B. W. (1995). Energetic origins of specificity of ligand binding in an interior nonpolar cavity of T4 lysozyme. *Biochemistry*, **34**, 8564–8575.
47. McKim, S. & Hinton, J. F. (1993). Xe-129 NMR spectroscopic investigation of the interaction of xenon with ions in aqueous solution. *J. Magn. Reson. ser. A*, **104**, 268–272.
48. Clever, H. L. (ed.) (1979). Solubility Data Series, vol. 2, Pergamon, New York.
49. Johnson, B. A. & Blevins, R. A. (1994). NMRView: a computer program for the visualization and analysis of NMR data. *J. Biomol. NMR*, **4**, 603–614.
50. Delaglio, F., Grzesiek, S., Vuister, G., Zhu, G., Pfeifer, J. & Bax, A. (1995). NMRPipe: a multidimensional spectral processing system based on UNIX Pipes. *J. Biomol. NMR*, **6**, 277–293.
51. Leslie, A. G. W. (1992). Recent changes to the MOSFLM package for processing film and image plate data. *Joint CCP4+ESF-EAMCB Newsletter on Protein Crystallography*, **26**.
52. Collaborative Computational Project Number 4 (1994). The CCP4 suite: programs for protein crystallography. *Acta Crystallog. sect. D*, **55**, 49–81.
53. Brunger, A. T., Adams, P. D., Clore, G. M., DeLano, W. L., Gros, P., Grosse-Kunstleve, R. W. *et al.* (1998). Crystallography and NMR system: a new software suite for macromolecular structure determination. *Acta Crystallog. sect. D*, **54**, 905–921.
54. Jones, T. A., Zou, J.-Y., Cowan, S. W. & Kjeldgaard, M. (1991). Improved methods for building protein models in electron density maps and the location of errors in these models. *Acta Crystallog. sect. A*, **47**, 110–119.
55. Laskowski, R. A., MacArthur, M. W., Moss, D. S. & Thorton, J. M. (1993). PROCHECK—a program to check the stereochemical quality of protein structures. *J. Appl. Crystallog.* **26**, 283–291.

Edited by P. Wright

(Received 9 May 2002; received in revised form 12 July 2002; accepted 15 July 2002)